Investigating Biomechanical Noise in Neuroblastoma Cells using the Quartz Crystal Microbalance

Abhinav Prasad[1], Anna Huefner[2,3], Sumeet Mahajan[3*], Ashwin A. Seshia[1*]

[1]Nanoscience Centre, Department of Engineering, University of Cambridge, 11 JJ Thomson Ave, Cambridge, CB3 0FF, United Kingdom

[2]Cavendish Laboratory, Department of Physics, University of Cambridge, 19 JJ Thomson Ave, Cambridge, CB3 0HE, United Kingdom

[3]Institute of Life Sciences, University of Southampton, Highfield, Southampton, SO17 1BJ, United Kingdom

[*]aas41@cam.ac.uk, s.mahajan@soton.ac.uk

KEYWORDS: Biomechanical noise, Quartz crystal microbalance, neuroblastoma cells, frequency stability.

SUMMARY

Quantifying cellular behavior by motility and morphology changes is increasingly important in formulating an understanding of fundamental physiological phenomena and cellular mechanisms of disease. However, cells are complex biological units which often respond to external environmental factors by manifesting subtle responses that may be difficult to quantify using conventional biophysical measurements. This paper describes the adaptation of the Quartz crystal microbalance (QCM) to the quantitative study of neuroblastoma cells under environmental stress wherein the frequency stability of the device can be correlated to changes in cellular state. By employing time domain analysis of the resulting frequency fluctuations studies of cellular motility and distinguishing between different cell states induced by applied external heat stress for the SH-SY5Y neuroblastoma cell line is possible. The changes in the frequency fluctuation data are correlated to phenotypical physical response recorded using optical microscopy under identical conditions of environmental stress. This technique provides a basis to quantify the associated biomechanical noise paving the way for its use in monitoring cell activity, and intrinsic motility and morphology changes, as well as those resulting from the action of drugs, toxins and environmental stress.

INTRODUCTION

Depending on the cell type and environment, cells often undergo continuous morphological and motility changes. Cytoplasm and sub-cellular components self-organize to change shape and also provide the basis for cellular motility. These processes, though superficially simple, are highly complex and represent nature's unique solutions to challenges posed by mechanics, thermodynamics and biochemistry. Diverse biological processes ranging from embryogenesis, fetal and organ development to immune response against inflammation and wound healing involve movement or migration of cells[1]. Cellular motility also plays a crucial role in many diseases including in tumor invasion and spread (metastasis) of cancer. Therefore understanding and targeting cell motility is a topical strategy in reducing morbidity and fatality in cancer treatment[2]. Cellular morphology also provides an indication of the conditions being experienced by the cells as well as that of the various biological processes operative in cells[3].

The attachment-detachment of cells to the underlying substrate and extra-cellular matrix (ECM) takes place through focal adhesion points which involve binding of integrin mediators to ECM molecules leading to the formation of focal complexes[4]. Integrin receptors are connected to cytoskeleton through actin networks which influence reorganization of cytoskeleton, hence, the cell structure itself[5]. These processes have biomechanical consequences and can be used to model the behavior of cells. Assuming environmental factors as input, cells (both individually and collectively) represent physical dynamical systems which respond to the input (stimuli) by modulating their motility and morphological characteristics. These biomechanical manifestations are often stochastic and, thus, call for a tool for sensing and interpretations. Techniques based on optical microscopy[6–8], micromanipulation[9], modified AFM[10] and optical traps[11] have been used to understand the mechanics of focal adhesion[12], however, analysis of stochastic aspects of cellular motility and morphology is missing. Thus, there is a need of development of a biomechanical noise probing technique that could be simple, non-invasive and real-time. In this paper, we use one of such techniques, based on Quartz Crystal Microbalance (QCM), to study

the biomechanical noise associated with human neuroblastoma cells.

In the past few decades, the Quartz Crystal Microbalance (QCM)[13] has emerged as an important tool for highly sensitive, label-free, gravimetric measurements of physical processes involving physical adsorption and desorption of a variety of analytes. The QCM can be mechanically abstracted as a single degree-of-freedom spring-mass-damper system such that any attachment/detachment of analyte on the crystal manifests in the form of a change in resonant response that is read out using external electronics. This property of QCM has been extensively used to perform measurements on biological systems in liquid environments. In the presence of liquid, acoustic oscillations of the QCM couple to the surrounding liquid media and the viscoelastic properties of the media at the interface[14] have predictable effects on the frequency (f) and dissipation (D) characteristics of the QCM. A range of biological systems have been probed using the QCM including the physi/chemi-sorption of proteins and lipids[15], binding and reaction kinetics of biomolecules[16], cell attachment-detachment and spreading[17–20] etc. Descriptive models [21,22] have been proposed to correlate adsorption-desorption and binding studies using the QCM but for complex systems such as cells, a quantitative description using conventional analysis ($f - D$) techniques is often inadequate. When such systems are influenced by actively driven dynamic and non-equilibrium processes like motility and morphological perturbations, fluctuations in the QCM response as a function of time are seen. There is, therefore, the possibility of utilizing the resulting recorded fluctuations in response as a means of characterizing such dynamic and complex biological systems.

It can be hypothesized that movement of cells on the surface can result in biomechanical noise that can couple to response of the QCM and be conspicuously evidenced in terms of enhanced levels of fluctuations in the recorded QCM response. Sapper *et al*[23] previously reported that the effect of biomechanical noise on frequency fluctuations in a QCM is several orders of magnitude higher than that contributed by other noise sources. By calculating the power spectral density (PSD) of the QCM frequency fluctuations in the case of attached mammalian cells, the authors were able to qualitatively associate frequency fluctuation data with cell motility. In a separate study, Tarantola *et al*[24] studied motility of different cancer cell lines using the same technique. In both the studies, outcome of the fluctuation analysis was compared with a similar analysis on the Electric Cell-Substrate Impedance Sensing (ECIS) data.

In the present paper, neuroblastoma cancer cells are studied using a time-domain fluctuation analysis technique (Allan Deviation measurements) applied to the measured QCM response. The case study of neuronal cells (from the differentiated human neuroblastoma cell line) is considered where their interactions with the sensor surface are monitored, while subjecting the cells to external heat stress which eventually leads to apoptosis. This study provides insight into the mechanical response of the particular type of cancer cells due to the change in local temperature. By combining separate optical studies with QCM data, it is possible to correlate the observed changes in single cell state and morphology as well as total surface coverage of the cells to the QCM frequency fluctuation data. Thus, the paper establishes the basis for the use of time-domain QCM frequency fluctuation analysis for sensing biomechanical noise output of cells, deciphering and monitoring physical behavior of cells and cell-substrate interactions and the changes induced due to environmental stress. The results indicate that this technique can be expanded to other case studies on cellular systems and the effect of varying environmental conditions on their mechanical behavior.

MATERIALS AND METHODS

A. QCM Set-up

AT-cut plano-plano thickness shear mode Cr/Au coated 5 MHz quartz crystals, 1 inch in diameter (see schematic in Fig. 1A) are used. Crystals were fitted into a dedicated Kynar® flow-cell, part of the standard QCM200® instrument from Stanford Research Systems (SRS). The flow-cell volume is approximately 150 µl. Crystal electrodes are isolated from the flow media and electrical connections to the interface electronics is achieved through spring-loaded contact pins. During experiments, the series resonance frequency and crystal resistance is logged and then later processed off-line. The gate-time (sampling time) of the instrument was set to 1 s. The temperature of the flow-cell was controlled by a heater with the whole set-up being placed inside an environmental chamber with fully humidified atmosphere at 37°C and 5% CO_2 during the length of the experiments on the live cells. The environmental chamber was placed on a vibration isolation table and the attached electrical cables, connecting the crystal to the measurement set-up (outside the chamber), were fitted with foam dampers at points of contact with the chamber to prevent external vibrations arising from the humidifier or other sources from impacting measurement.

B. Cell-culture and crystal chip preparation

Experiments were carried out using SH-SY5Y cells, a human neuroblastoma cell line, commonly used to study neuronal function and behavior[26]. Cells were adherent with neurite outgrowth. Moreover, the cells tended to grow in clusters resulting in patchy surface coverage of the culture dish. Cells were cultured at 37°C in humidified atmosphere in a medium containing 87% Dulbecco's Modified Eagle's Medium (GIBCO), 10% heat inactivated fetal bovine serum (PAA), 2% B-27® (GIBCO) and 1% antitibiotic-antimycoticum (GIBCO). The addition of 10 nM staurosporine (Sigma) to the culture medium triggered cell differentiation into a neuroblast-like cell type, which arrests proliferation and results in a stable population[27]. The cells studied in this work do not undergo cell division but nevertheless change their shape both as a result of movement and environmental stress[28,30,31]. Thereafter,

a required number of cells were reseeded on autoclaved, poly-L-lysine (PLL, Sigma) coated quartz crystals placed inside a 35 mm culture dish (Greiner). Prior to the seeding of cells the quartz crystals were incubated with aqueous PLL (0.02 m/v %) solution for two hours at 37°C to facilitate adherence of cells to the surface. A schematic of a cell attached to a PLL-coated quartz crystal is shown in Fig 1B.

In order to study cell motility, the number of cells seeded on the quartz crystal should result in a relatively sparse coverage to minimize the influence of cell compression and contact inhibition[28]. Therefore, two extreme cell concentrations were chosen to study cell behavior and motility. Approximately 5,700 cells per cm^2 and 51,700 cells per cm^2 were seeded onto the quartz crystal containing cell culture dishes. These seeding densities resulted in a surface coverage of ~3.6% (surface coverage i) and ~30.7% (surface coverage ii), respectively, which was measured by quantifying the cell population over a relatively large area (~0.5 cm^2) of the quartz crystal using optical images to remove the influence of local heterogeneity due to cell colonies/clusters. Experiments for intermediate surface coverages, 13.0% (surface coverage iii) and 22.5% (surface coverage iv) along with control experiments were also performed. Cells were allowed to attach to the substrate over 24hrs. Thereafter, cell attachment and viability was checked using a light microscope.

Crystals demonstrating good attachment of cells on the surface were then chosen for individual experiments. These crystals were placed inside the pre-warmed flow-cell which was filled with cell culture medium carefully avoiding introduction of air bubbles, which can interfere with the QCM readings. The flow-cell was sterilized with 70% ethanol prior to cell experiments and thereafter kept under sterile cell culture conditions to exclude contamination of the cells throughout the experiments. The flow-cell was then placed inside the environmental chamber, connections to electronics were made, and data recording with the QCM was initiated after an initial stabilization period of ~20 min. During QCM measurements there was no flow of the medium to preclude flow-related perturbations.

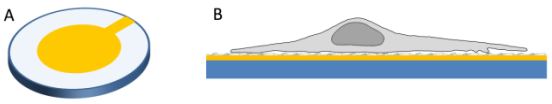

Figure 1. (A) Schematic of a quartz crystal Cr/Au top-surface electrode (yellow), and **(B)** Cross-sectional schematic view of a SH-SY5Y human neuroblastoma cell adhering to the poly-L-lysine (PLL) coated crystal. (*Relative dimensions not to scale*)

C. Hyperthermia induced, time-lapse live cell experiments

Changes in cellular morphology and motility were studied in SH-SY5Y cells seeded onto a 35 mm glass-bottom dish (Mattek, USA) with a surface coverage of ~30.7%. Hyperthermia was induced by gradual temperature increase from 37 °C to 45 °C in an environmental chamber (humidified atmosphere with 5% CO2) of a Leica microscope allowing for live cell, time-resolved phase-contrast imaging using a 40x objective. Time-lapse recording was started simultaneously with the initiation of temperature increase. The temperature was measured in the air chamber and a final temperature of 45 °C was recorded after 50 minutes. Time-lapse video recording was carried out capturing one frame every 20 seconds. For cell tracking, image sequences were pre-processed using threshold adaptation, background subtraction, followed by using an unsharpening mask and binarization in ImageJ (NHI, USA)[29]. For every frame, boundaries were drawn using the marking tool in ImageJ and shape parameters like centroid, area and circularity were obtained. Centroid positions were superimposed on the optical frames to visualize the track of selected cells and further processing on the data was performed to calculate distance travelled, mean squared displacement and speed.

RESULTS AND DISCUSSION

A. Heat stress experiments

Cell covered QCM crystals were prepared as detailed earlier (Materials and Methods) and loaded into the flow chamber. After the recordings on the QCM crystal stabilized, the temperature of the heater was ramped up from 37 °C to 45 °C. This change in temperature induces stress resulting in changes in the cell shape and texture indicating apoptotic processes and ultimately resulting in apoptosis (as shown in the later sections). Data was recorded beyond the time after the temperature monitor (attached to the exterior of flow cell) reached the final set temperature to allow for equilibration and compensate for any thermal lag. After every experiment, the crystals were viewed under the microscope to confirm that the cells have undergone apoptosis triggered by the heating process and formed typical spherical shapes alongside with detachment from the surface. Frequency data for two such experiments are shown in Fig. 2(A). As the temperature was increased, both crystals showed a gradual positive frequency shift (ΔF) indicating a change in mass loading (Δm) on the surface. Frequency shift for the larger cell population (~250 Hz) is much greater than the one observed in the case of the smaller cell population (~50 Hz) as expected roughly from the Sauerbrey equation ($\Delta F = -2{F_0}^2 \Delta m / A\sqrt{\rho_q \mu_q}$, where F_0, A, ρ_q, μ_q are the un-

loaded crystal resonance frequency, active crystal area i.e.

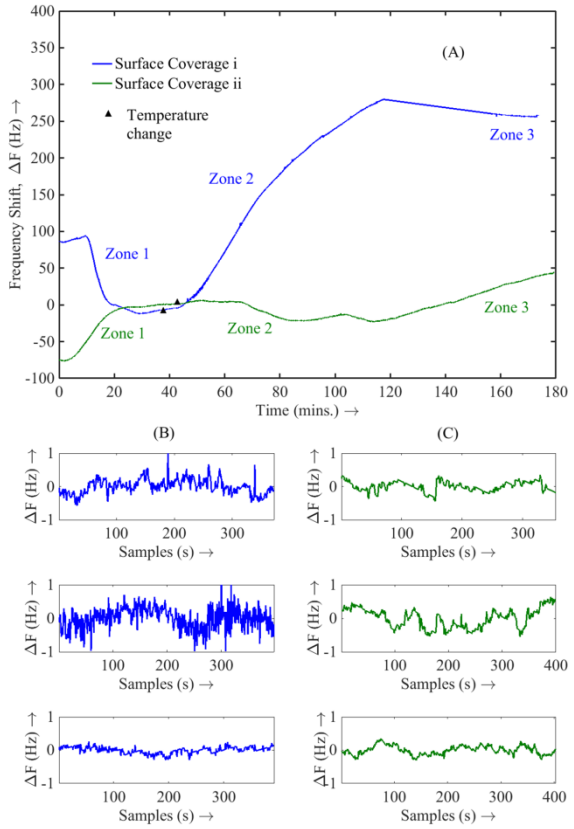

Figure 2. (A) Frequency shift plots for two different surface coverages: 3.6% (surface coverage i) and 30.7% (surface coverage ii) of SH-SY5Y human neuroblastoma cells on different quartz crystals. Markers indicate the point of commencement in temperature increment of the flow-cell from 37 °C to 45 °C in order to apply heat shock to the adherent cells. Three different zones are also annotated roughly defining three different stages of the experiments. Zone 1 is where cells are healthy, Zone 2 is immediately after the temperature is increased and represents transition to cell apoptosis while Zone 3 is the stage just before the experiment is concluded with final stages of apoptosis. Increase in frequency in both the cases indicates decrease in mass loading (i.e. cell detachment from the surface) with time. **(B)-(C)** (*Two columns of three plots each*) are snapshots of frequency fluctuations in Zone 1, Zone 2 and Zone 3 (*top to bottom*) for the two cases of varying surface coverage. In all cases, the trend-line has been adjusted for representation purposes only. Notice that in the case of larger surface coverage, the signal is more "noisy" in Zone 2 while it is least in Zone 3. In the case of lower surface coverage, differences in the frequency fluctuations in three different zones are relatively smaller than the former case.

area constrained by the electrodes, density of quartz and shear modulus of quartz respectively). It should be noted that the Saurbrey equation has limited validity in this case and a more elaborate model is necessary for quantitative correlation to the experiment due to the complex nature of the physical system under investigation. While accurate prediction of changes based on frequency data alone is challenging due to the complex nature of the interfacial surface, the changes could be qualitatively interpreted as due to rupture of strong adhesion bonds of cells, as they progress towards apoptosis, which are slowly replaced by loose physisorption, both for the cells which remain on the surface and those that sink after complete detachment. This observation is consistent with previous experiments on studying cell apoptosis using the QCM[36].

B. Biomechanical noise and frequency fluctuations

Frequency and dissipation readings provide valuable information on changes occurring at the crystal-liquid interface and have proven to be especially useful in ligand binding experiments. While cell adhesion, spreading, detachment and morphological changes in presence of an analyte have been previously studied by QCM using the frequency-dissipation approach[18–20,37] dynamic changes or fluctuations in these parameters have been given little attention. Fluctuations in QCM parameters have been shown to correlate with the subtle changes in mass and viscous loading at the interface[23,24]. Cell-substrate interactions probed using the QCM involve constant attachment and detachment at focal adhesion points, morphological changes and cell-cell interactions which can result in perturbations in viscoelastic loading on the QCM. These variations, representing biomechanical noise contribution of the seeded cells, are recorded as frequency fluctuations in the QCM data.

Based on QCM frequency measurements, three zones are defined on the basis of variability in environmental and interfacial conditions. Zone 1 is defined as the time period starting from the point where data recording is commenced and the system is held at 37°C. This zone corresponds to the case where cells are viable and kept in ideal culture conditions. Zone 2 is defined as the zone starting immediately after the temperature is increased and up to the point where all cells are in the late stages of apoptosis due to hyperthermia. Zone 3 is defined as the region where the environment has reached the final phase following cell death due to the heat shock treatment in Zone 2. The frequency fluctuation data for both experiments is plotted in Fig. 2(B)-(C). It is clear, even by visual examination, that the amplitude of frequency fluctuations is reduced significantly for Zone 3 compared to Zone 1 for higher cell coverage. An increased amplitude of frequency fluctuations indicates large scale activity on the surface, which is to be expected when the cells are healthy and mostly stable in clusters (colonies) compared to when they are largely static (apoptotic). Both frequency shift and fluctuation amplitude changes for the smaller surface coverage are relatively indistinguishable and do not shed much light qualitatively. However, to establish more quantitative insight into these observations, time-domain frequency stability analysis is employed.

C. Time-domain Biomechanical Noise Analysis

Two sample Allan Deviation

Frequency fluctuations (hence, biomechanical noise) can be characterized either by performing frequency domain analysis (calculating power spectral density (PSD)) of the data or by analyzing the Allan variance in time do-

main. Though inter-convertible, Allan variance is chosen over PSD as it is more convenient to interpret in terms of the experimental set-up used in this work, which due to use of a frequency counter, outputs observed frequency as a time series. A complete PSD based analysis for the experiments is also provided in the Supplementary Information to provide a comparison with previous studies.

A quantitative measure of frequency stability is established by analyzing the Allan variance (see Supplementary Information) for the data sets corresponding to the various cases of cell coverage in Zones 1-3. The Allan variance is chosen over standard M-sample variance as it is convergent for most types of noise processes and can help distinguish different noise mechanisms as well. An overlapped Allan variance, $\sigma^2{}_y(\tau)$, for M fractional frequency values, is employed to provide higher statistical confidence (see Supplementary Information).

Plots showing overlapped Allan deviation as a function of averaging time show a power-law dependence as a function of averaging time (τ) with characteristic slopes $\mu(\sigma_y(\tau) \sim \tau^{\mu/2})$ in such plots and, thus, can be readily identified. White noise (f^0) describes $\mu = -1$, Flicker noise ($1/f$) describes $\mu = 0$, Random walk frequency modulated noise ($1/f^2$) describes $\mu = 1$, while frequency drift describes $\mu = 2$[38,39]. While the frequency fluctuation data shown in Fig. 2 is linear drift compensated, there is no pre-processing of the frequency fluctuation data used to calculate overlapped Allan deviation. Further, error estimates for 1-sigma confidence intervals are calculated for all the three zones. Fig. 3(a) shows the sigma-tau plot for the high surface coverage cell experiment where the difference between the Allan deviation values (fluctuation levels) for three different zones is very clear. This agrees well with the frequency fluctuations observed in the three zones. Further, the deviation plot for each zone is considered separately and slopes between every pair of adjacent points are obtained using linear fitting. Relevant plots are shown in Fig. 3 (A)-b,c,d. Similarly, Fig. 3(B) represents sigma-tau plots for the low cell surface coverage. In this case, for short averaging times, the Allan deviation values are very close to each other while they diverge a bit for longer averaging times.

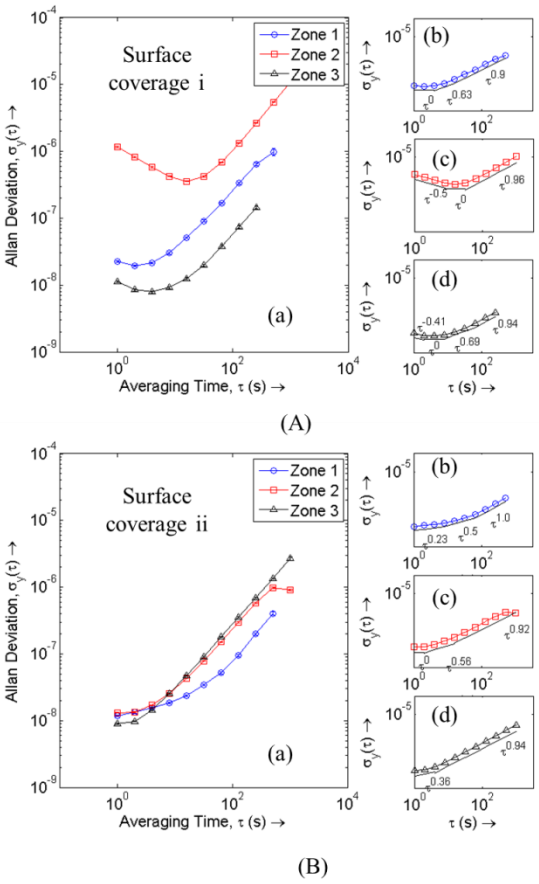

Figure 3. (A)-(B) Log-log overlapped Allan-deviation plots for the larger and smaller surface coverage cases respectively. From **(A)-(a)** it is quite evident that the fluctuation levels for all averaging times ($\boldsymbol{\tau}$) are highest for Zone 2, intermediate for Zone 1 while levels are lowest for Zone 3. This indicates when cells are alive, due to their activity, fluctuation levels are higher as compared to when cells are dead. Also, when cells are in a stressed state higher fluctuation levels are observed. **(A)-(b-d)-** Individual linear fitting curves (*black, continuous and slightly offset for clarity*) for three zones. Similarly, from **(B)-(a)** it is evident that while fluctuation levels for shorter averaging times are higher for both Zone 1 and Zone 2 relative to Zone 3 but between Zone 1 and Zone 2, fluctuation levels are only slightly higher for Zone 2. Linear fitting (**b-d**) indicate nature of noises (power-law type) for different zones as in the former case.

Interpretation of log-log overlapped Allan deviation plots

Individual deviation values for each time factor is calculated and can be used to compare the fluctuation levels between different zones. In Table 1, deviation values for shortest averaging time (1s) are used for representation. In the case where cells are cultured on the QCM, it is quite evident that deviation values are the maximum for Zone 2, are the least for Zone 3 and lie in-between these two values for Zone 1. The relative difference between deviation values is clear between high and low surface coverage of cells. In all the cases though, for Zone 3, fluctuation values are $\simeq 10^{-8}$ which approximately corresponds to the baseline fluctuation level. To determine the effect of heating on the fluctuation levels, two control experiments, without any cells, were performed with,

first, just water and, secondly, with the cell culture medium. All other conditions were kept the same. Log-log plots of deviation values for the control experiments are shown in Fig 4 (C)-(D). Clearly there is very little change in the fluctuation levels when the temperature is increased implying that the observed noise levels (Fig 4A-B) are generated due to the presence of the cells on the surface. Experiments with intermediate cell coverage of 13.0% (surface coverage iii) and 22.5% (surface coverage iv) were also performed. Both the experiments agree with the trends in the frequency fluctuation data observed with the high and low surface coverage experiments. For averaging factors $\tau = 2\ s, 4\ s$, a similar table can be formulated to provide similar trends (see Supplementary Information). For larger averaging times ($\geq 8\ s$), the plots start to intersect pointing towards the fact that values must be interpreted with care. To understand the contribution of different noise sources at various time scales, we can separate the contribution of device noise from the biomechanical noise emerging from the activity of the cells themselves by comparison with respect to control experiments. Some of the principal device noise could be evidenced as thermal noise or flicker noise with noise contributions from the crystal and the amplifier, along with sensor drift due to changes in environmental conditions. Physical processes associated with cellular activity such as attachment-detachment of individual focal contacts, morphological changes in response to external environmental conditions and internal cellular processes, migration of cells on the surface, cluster dynamics of cells, fluctuations in the viscoelasticity of the fluid due to cell activity and external environmental perturbations are expected to contribute to the measured frequency fluctuations. Each of the above processes are expected to operate on different time scales, for example, attachment-detachment between extracellular matrix and cells are much faster (t_{off}^{0} for spontaneous dissociation of a closed bond at a focal adhesion site can range from fraction of seconds to tens of seconds[40]) while motility and cluster dynamics can be relatively slower. As shape changes are sensitive to external conditions, any fast external processes are going to influence the cell morphology at a similar rate. A plot of Allan deviation slopes for different averaging times can be found in the Supplementary Information. Nevertheless, in order to correlate and verify predictions from the time-domain frequency analysis with cell behavior optical imaging experiments were carried out.

Table 1. Two sample overlapped Allan deviation values at $\tau = 1\ s$ for different zones and varying surface coverage

Experiment	Zone 1 (10^{-8})	Zone 2 (10^{-8})	Zone 3 (10^{-8})
Surface coverage i (30.7%)	2.248	116.2	1.122
Surface coverage ii (3.6%)	1.172	1.310	0.899
Surface coverage iii (13.05%)	2.31	3.2	1.024
Surface coverage iv (22.5%)	1.67	99.186	1.612
Control-DI Water	0.861	0.865	0.742
Control-Cell Culture	0.975	0.888	0.742

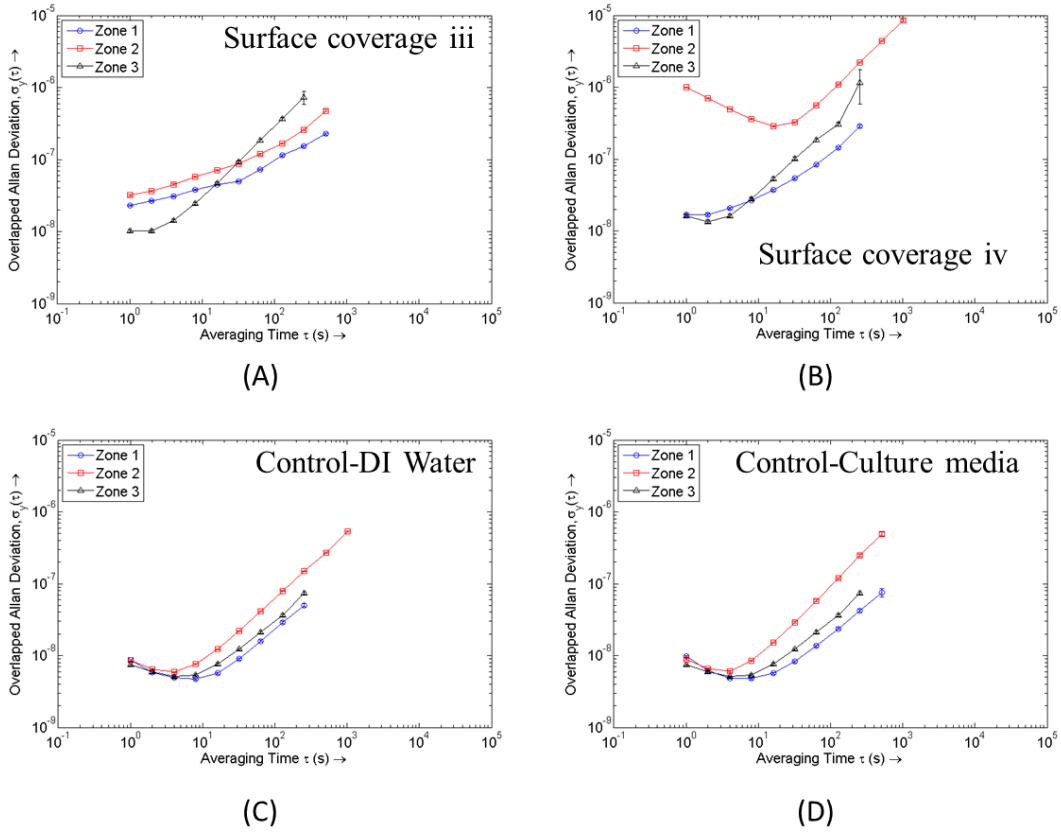

Figure 4. (A)-(B) Log-log Overlapped Allan-Deviation plots for surface coverage iii (13%) and iv (22.5%) while **(C)-(D)** are Overlapped Allan-Deviation plots for control experiments. All the steps are common in the control experiments with the exception of absence of any seeded cells. In **(C)**, surrounding media is DI water while in **(D)** surrounding media is cell culture.

D. Correlating frequency fluctuation data with optically recorded cellular mechanical behavior

Observing a sample cell

The aim of this section is to correlate the frequency fluctuation analysis with cellular changes and behavior in terms of motility, substrate adhesiveness and morphology resulting from hyperthermia. Therefore, cells were exposed to increasing temperature under conditions comparable to those used during the QCM experiment and optical images were obtained using a phase-contrast microscope to extract information on morphology and motility.

Fig 5 (A)-(H) shows eight selected time points for the same cell sample exemplifying the drastic cellular changes due to hyperthermia. The position of the same cell which moves on the surface and changes in morphology is marked with a star/asterisk (*). Significantly, the size of the nucleus increases on increasing the temperature and thereafter, the nucleus shrinks (Fig 5 (E)-(F)) until distinction from the cytoplasm is not possible any more (Fig 5 (G)-(H)). Furthermore, pigmentation of the nucleus becomes uneven showing darker spots as visible in Fig 5 (C)-(H). Nuclear swelling and chromatin aggregation have been observed in the context of apoptosis induced hyperthermia[43,44]. In the same images, similar abnormal coloration of the cytoplasmic region is observed that is likely triggered by the aggregation and rearrangement of cytoskeletal proteins caused by the heat treatment. Several other changes in the morphology can be seen including reduced branching of neurites and blebbing (bubble-shaped protrusions) as highlighted by the white arrows in Fig 5 (F)-(G). The cell size sharply decreases after prolonged heat treatment as seen in Fig 5 (E)-(H) with gradual rounding the cell shape indicating apoptosis and ultimate detachment from the surface indicated by halo around each cell.

Cell tracking analysis

For further quantification of cellular movement during heat stress treatment, we performed cell tracking analysis. Fig 6 (A), (B) and (C) represent the frames recorded at the beginning, during and end of the optical imaging experiment, respectively. Individual cell movement tracks are labeled and colored in the frames. One clear observation from cell tracking is that the motion of cells changes from being directed (elongating and reaching out in a particular direction) with nearly linear displacement track to-

wards localized, confined movement. This change occurs simultaneously with the change in cell shapes outlined in the previous section.

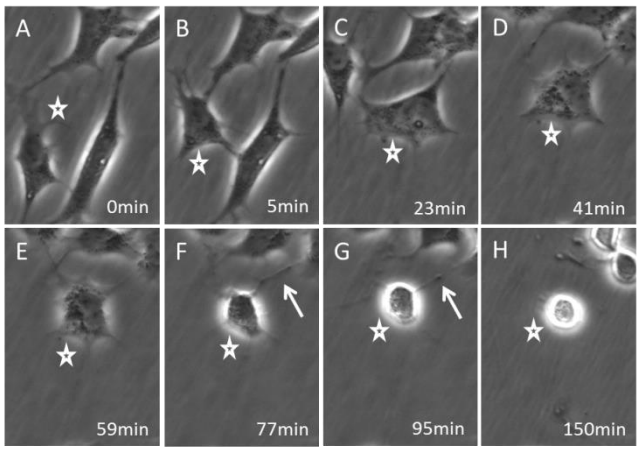

Figure 5. (A)-(H) Phase-contrast optical images of cells seeded on a PLL coated glass surface. Temperature is gradually increased from 37°C to 45°C over a period of 150 min during which cells change morphology, ultimately shrink in size and become round which is characteristic of apoptosis.

To identify the movement of cells during the heat stress stage of the experiment, mean-square displacement (MSD) for each cell is calculated using the following expression for two dimensional motion:

$$MSD(\Delta t) =< (\Delta r)^2 >= \quad (1)$$
$$< \big(x(t) - x(t+\Delta t)\big)^2$$
$$+ \big(y(t) - y(t+\Delta t)\big)^2$$

where, x(t), y(t) are spatial position loci of a cell. By plotting the MSD vs Δt, the motion can be characterized as either confined random walk (Fig 6 (D)) using $MSD(\Delta t) = 4D\Delta t^{\alpha}$ or as a superposition of directed motion and diffusion using $MSD(t\Delta) = 4D\Delta t + (v\Delta t)^2$ where, D is the diffusion constant and α<1. During the first 16mins of the time-laps experiment, the temperature was not observed to increase more than 0.2°C and allows us to assume that cells are exposed to normal culture conditions. Cell motility was characterized during this phase to make following heat-induced changes apparent and comparable. Roughly, two groups of cells were identified, one with faster motility and directed motion ($v \sim 1.5 \mu m/min$), while the other shows a slower movement ($v \sim 0.38\ \mu m/min$) with a diffusion constant of $D \sim 2 * 10^{-2}\ \mu m^2 s^{-1}$ for both. These observed motilities take cell-cell interactions into account which slows down the overall speed and causes observed differences between the groups.

As discussed before, cellular motility depends on many environmental factors such as temperature, cell culture medium[34] and substrate properties such as rigidity, microstructure[41] and coating[33] as well as being dependent on the cell type or cell line and the seeding density. In particular, it has been shown that cellular confluency influences cellular behavior and cell morphology as higher cell densities compromise the individual cell area impacting on cell morphology and motility[42]. Many intracellular processes are involved in cell migration. In the direction of cell migration, a leading edge is formed by extending flat membrane processes composed of an inner actin crisscross network called lamellar ruffling. This is accompanied by the cell-substrate interactions in order to form adhesion points at the leading processes. Then, the cell body, including cytoplasm and organelles, is shifted while the trailing cell rear is retracted. Thereby, temperature affects cell motility and related characteristics such as lamellar ruffling protrusion as shown by Shelden *et al* [31] for human neuroblastoma cells. Lamellar ruffling has been observed to increase for temperatures up to 40°C (mild hyperthermia) but declines for further temperature increase. Furthermore, Hartmann-Petersen *et al*[34] have studied cellular process domains as well as mean cell speed and area in murine fibroblasts under temperature conditions of 37 to 40°C and demonstrated an increase of characteristic values proposing the assumption that cells at slightly higher temperatures are more spread out and motile.

Similar observations have been made for the cell motility of 3T3 cells showing a peak between 36.5 to 38.5°C, with strongly declining motility towards lower or higher temperatures[43]. It is commonly known that prolonged treatment of cells at hyperthermic temperatures compromises cell viability and effectively triggers apoptosis. Treatment of cells with temperatures as high as 43°C for at least one hour has been shown by Luchetti *et al*[44] to already trigger apoptosis in human neuroblastoma cells. This is accompanied by changes in cell morphology such as blebbing, nuclear swelling, chromatin margination and changes in the cell shape eventually followed by cell rounding. Cytoskeletal proteins undergo aggregation and rearrangements leading to the final breakdown of microtubules. Additionally, cellular membrane characteristics are altered leading to cellular adhesiveness impairment[45,46].

The observed motility of cells along with the constant morphological readjustments within and around clusters continuously varies the viscoelastic loading of the QCM and contributes to the fluctuations in resonant frequency observed. Even when cells are observed under healthy and stable conditions, there is constant motility contributing to the variations in resonance frequency. Thus, as cells are stressed, their motility increases initially and then drops. Further, during the final part of the experiment, the remaining small and round cell bodies appear to describe random motion. To quantitatively characterize this cellular motion in order to find out whether this motion could contribute to the noise levels, images from 120 frames between 150th and 190th minute were used. Fitting the tracking data to the above equations revealed that cells have a diffusion constant of $\sim 10^{-2} - 10^{-3}\ \mu m^2 s^{-1}$ indicative of Brownian motion (Fig 6 (E)). This confirms the hypothesis of cellular detachment as the temperature increases. Thus, following the final stages of apoptosis, cells are eventually either loosely attached or

completely detached. The detached cell body is located above the penetration depth region, which accounts for the reduced fluctuations observed in Zone 3 in the QCM experiments.

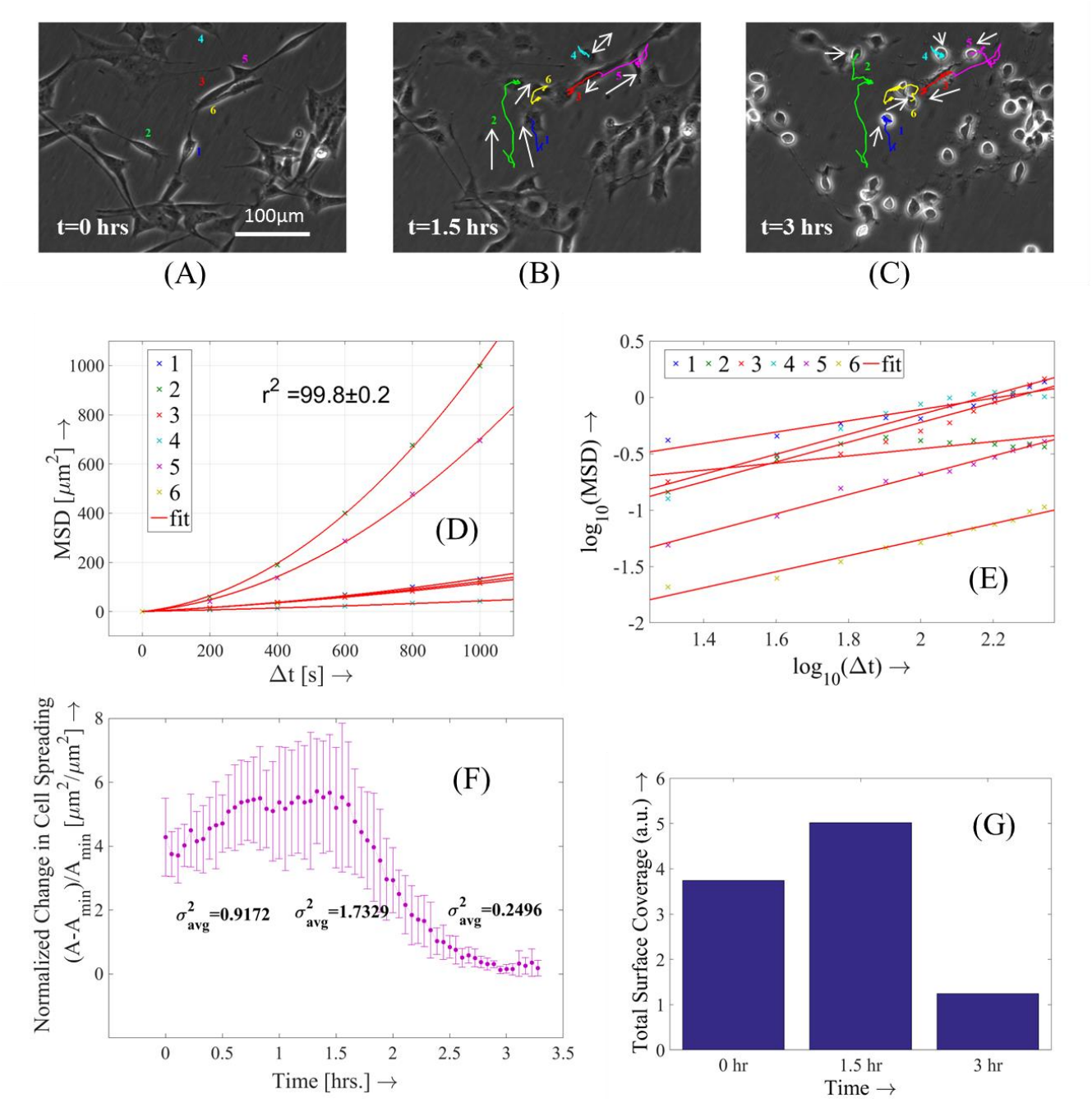

Figure 6. (A)-(C) Phase-contrast optical images of SH-SY5Y cells at different time instances during the heating process. Coloured lines represent the tracks of various cells undergoing heat induced stress. In **(B)** arrows are indicating the direction of motion of individual cells while in **(C)** they are indicating the final position of the cells. **(D)** Mean-square displacement plots of cells prior to the heat-stress phase of the experiment (first 16 minutes) indicating the presence of at least two categories of cells movements, fast and slow, while, a close fit to $\boldsymbol{MSD(\Delta t) = 4D\Delta t + (v\Delta t)^2}$ is performed to extract diffusion coefficients and speed values. Similarly, **(E)** is MSD log-log plot for the last stage of the experiment (150th-190th minute). **(F)** Mean and standard deviation values for normalized change in cell spreading (*apparent overlap* area) area of the cells under consideration are plotted against time which peak almost half way through and then rapidly decrease until the cells become spherical. **(G)** Total surface coverage shows a similar trend.

Apart from the cell motility data, another observable factor that correlates well with the fluctuation analysis is the cellular spreading obtained from the apparent cellular overlap area. To calculate the relative change in the spreading, we normalize instantaneous apparent overlap area with respect to final apparent overlap area where

sphericity is observed for each cell. The procedure is repeated for the whole sample set and mean and standard deviation values were calculated for the recorded frames. From Fig 6 (F), it is quite evident that, cellular spreading reaches a maximum midway and this is also where maximum deviation values are observed. Depending on the immediate vicinity and state of the cells, some show a larger change in spreading while others do not. As the cells undergo apoptosis, we observe almost uniform overlap area across the sample set with reduced deviation values. Cells attach to surfaces through focal adhesion points and therefore a change in the spreading is likely to result in the increase of these focal contact points, leading to larger perturbations per cell. Also as the spreading changes, viscoelastic loading near the QCM surface will also change. All this effectively changes the loading conditions of the QCM. It is clear from the calculations that the total surface coverage (Fig 6 (G)) increases by 34% first as the temperature increases and eventually decreases by 67% (relative to the initial surface coverage).

Both the motility and morphological data obtained from parallel optical experiments strongly correlate with the fluctuation analysis of QCM signals. The prediction from the fluctuation analysis that on heating an initial increase in fluctuations is a result of increase in activity as proved by the concomitant increase in motility and contact area (morphology change) observed in optical experiments. Similar observations of increased motility on slight increase of temperature before declining in another cell line[43] boost the validity of our time-domain fluctuation analysis. Overall the fluctuation analysis and its classification into the three different zones map directly to the cell state induced by thermal stress.

CONCLUSION

Understanding motility and cell behavior in response to stress is vital for many physiological processes and diseases. Cell motility and morphology are important measurable facets of cellular biomechanics while also being correlated with several underlying biochemical processes. These processes are also indicative of the physical state of the cell, and, any variations in the state induce variation in the biomechanical activity of the cell, often, describing apparently stochastic behaviour. In this work we have studied the motility and cell behavior of living neuroblastoma cells and the effects of thermal stress on them by QCM. Time-domain frequency fluctuation analysis is employed to provide insight into the complex behavior of neuroblastoma cells and this data is optically correlated to changes in motility and morphology. The fluctuation analysis reveals three distinct types of behavior which included the prediction of an increased state of activity of cells following an increase of temperature before a decrease of activity on account of cell death. Furthermore, the experiments provide interesting insight into the nature of cell-substrate interactions under healthy conditions and in response to thermal stress. The high degree of correlation between the frequency fluctuation data and optically recorded mechanical behavior also provides the basis for future studies using the QCM as a means of inferring the nature of physical processes underlying cell-substrate interactions by quantifying the associated biomechanical noise.

REFERENCES

1. Franz, C. M., Jones, G. E. & Ridley, A. J. 2002 Cell Migration in Development and Disease. *Dev. Cell* **2**, 153–158. (doi:10.1016/S1534-5807(02)00120-X)

2. Wells, A., Grahovac, J., Wheeler, S., Ma, B. & Lauffenburger, D. 2013 Targeting tumor cell motility as a strategy against invasion and metastasis. *Trends Pharmacol. Sci.* **34**, 283–9. (doi:10.1016/j.tips.2013.03.001)

3. Ingber, D. E. 2003 Tensegrity I. Cell structure and hierarchical systems biology. *J. Cell Sci.* **116**, 1157–1173. (doi:10.1242/jcs.00359)

4. Mattila, P. K. & Lappalainen, P. 2008 Filopodia: molecular architecture and cellular functions. *Nat. Rev. Mol. Cell Biol.* **9**, 446–54. (doi:10.1038/nrm2406)

5. Brakebusch, C. & Fässler, R. 2003 The integrin-actin connection, an eternal love affair. *EMBO J.* **22**, 2324–33. (doi:10.1093/emboj/cdg245)

6. Moustafa, Y., Chancel, J., Rossetti, F., Montmasson, M. P. & Idelman, S. 1992 Image analysis of lymphoid cell differentiation in rat thymus throughout development. *Thymus* **19**, 127–44.

7. Belmont, L. D., Hyman, A. A., Sawin, K. E. & Mitchison, T. J. 1990 Real-time visualization of cell cycle-dependent changes in microtubule dynamics in cytoplasmic extracts. *Cell* **62**, 579–589. (doi:10.1016/0092-8674(90)90022-7)

8. Sierra-Valdez, F. J., Cisneros-Mejorado, A. J., Sánchez Herrera, D. P. & Ruiz-Suárez, J. C. 2012 A thermal study of cellular motility by optical time-resolved correlation. *Rev. Sci. Instrum.* **83**, 044302. (doi:10.1063/1.3700248)

9. Marcy, Y., Prost, J., Carlier, M.-F. & Sykes, C. 2004 Forces generated during actin-based propulsion: a direct measurement by micromanipulation. *Proc. Natl. Acad. Sci. U. S. A.* **101**, 5992–7. (doi:10.1073/pnas.0307704101)

10. Parekh, S. H., Chaudhuri, O., Theriot, J. A. & Fletcher, D. A. 2005 Loading history determines the velocity of actin-network growth. *Nat. Cell Biol.* **7**, 1219–23. (doi:10.1038/ncb1336)

11. Footer, M. J., Kerssemakers, J. W. J., Theriot, J. a & Dogterom, M. 2007 Direct measurement of force generation by actin filament polymerization using an optical trap. *Proc. Natl. Acad. Sci. U. S. A.* **104**, 2181–6. (doi:10.1073/pnas.0607052104)

12. Gao, H., Qian, J. & Chen, B. 2011 Probing mechanical principles of focal contacts in cell-matrix adhesion with a coupled stochastic-elastic modelling framework. *J. R. Soc. Interface* **8**, 1217–32. (doi:10.1098/rsif.2011.0157)

13. Sauerbrey, G. 1959 Verwendung von Schwingquarzen zur Wagung dunner Schichten und zur Mikrowagung. *Zeitschrift fur Phys.* **155**, 206–222. (doi:10.1007/BF01337937)

14. Martin, S. J., Granstaff, V. E. & Frye, G. C. 1991 Characterization of a Quartz Crystal Microbalance with Simultaneous Mass and Liquid Loading. **2281**, 2272–2281.

15. Muratsugu, M., Ohta, F., Miya, Y., Hosokawa, T., Kurosawa, S., Kamo, N. & Ikeda, H. 1993 Quartz crystal microbalance for the detection of microgram quantities of human serum albumin: relationship between the frequency change and the mass of protein adsorbed. *Anal. Chem.* **65**, 2933–2937. (doi:10.1021/ac00068a036)

16. Hengerer, A., Kösslinger, C., Decker, J., Hauck, S., Queitsch, I., Wolf, H. & Dübel, S. 1999 Determination of phage antibody affinities to antigen by a microbalance sensor system. *Biotechniques* **26**, 956–60, 962, 964.

17. Wegener, J., Seebach, J., Janshoff, a & Galla, H. J. 2000 Analysis of the composite response of shear wave resonators to the attachment of mammalian cells. *Biophys. J.* **78**, 2821–33. (doi:10.1016/S0006-3495(00)76825-1)

18. Hong, S., Ergezen, E., Lec, R. & Barbee, K. a 2006 Real-time analysis of cell-surface adhesive interactions using thickness shear mode resonator. *Biomaterials* **27**, 5813–20. (doi:10.1016/j.biomaterials.2006.07.031)

19. Li, F., Wang, J. H.-C. & Wang, Q.-M. 2007 Monitoring cell adhesion by using thickness shear mode acoustic wave sensors. *Biosens. Bioelectron.* **23**, 42–50. (doi:10.1016/j.bios.2007.03.018)

20. Zhou, T., Marx, K. a, Dewilde, A. H., McIntosh, D. & Braunhut, S. J. 2012 Dynamic cell adhesion and viscoelastic signatures distinguish normal from malignant human mammary cells using quartz crystal microbalance. *Anal. Biochem.* **421**, 164–71. (doi:10.1016/j.ab.2011.10.052)

21. Yang, M. & Thompson, M. 1993 Multiple chemical information from the thickness shear mode acoustic wave sensor in the liquid phase. *Anal. Chem.* **65**, 1158–1168. (doi:10.1021/ac00057a010)

22. Ferreira, G. N. M., da-Silva, A.-C. & Tomé, B. 2009 Acoustic wave biosensors: physical models and biological applications of quartz crystal microbalance. *Trends Biotechnol.* **27**, 689–97. (doi:10.1016/j.tibtech.2009.09.003)

23. Sapper, A., Wegener, J. & Janshoff, A. 2006 Cell motility probed by noise analysis of thickness shear mode resonators. *Anal. Chem.* **78**, 5184–91. (doi:10.1021/ac060094g)

24. Tarantola, M., Marel, A.-K., Sunnick, E., Adam, H., Wegener, J. & Janshoff, A. 2010 Dynamics of human cancer cell lines monitored by electrical and acoustic fluctuation analysis. *Integr. Biol. (Camb).* **2**, 139–50. (doi:10.1039/b920815a)

25. Pax, M., Rieger, J., Eibl, R. H., Thielemann, C. & Johannsmann, D. 2005 Measurements of fast fluctuations of viscoelastic properties with the quartz crystal microbalance. *Analyst* **130**, 1474–7. (doi:10.1039/b504302f)

26. Biedler, J. L., Roffler-Tarlov, S., Schachner, M. & Freedman, L. S. 1978 Multiple Neurotransmitter Synthesis by Human Neuroblastoma Cell Lines and Clones. *Cancer Res.* **38**, 3751–3757.

27. Hong-rong, X., Lin-sen, H. & Guo-yi, L. 2010 SH-SY5Y human neuroblastoma cell line: in vitro model of dopaminergic neurons in Parkinson's disease. *Chin. Med. J. (Engl).* **123**, 1086–1092.

28. Meyer, G. E., Shelden, E., Kim, B. & Feldman, E. L. 2001 Insulin-like growth factor I stimulates motility in human neuroblastoma cells. *Oncogene* **20**, 7542–50. (doi:10.1038/sj.onc.1204927)

29. Schneider, C. A., Rasband, W. S. & Eliceiri, K. W. 2012 NIH Image to ImageJ: 25 years of image analysis. *Nat. Methods* **9**, 671–675. (doi:10.1038/nmeth.2089)

30. Mogilner, A. & Keren, K. 2009 The shape of motile cells. *Curr. Biol.* **19**, R762–71. (doi:10.1016/j.cub.2009.06.053)

31. Shelden, E. A. & Feldman, E. L. 2000 Automated difference image analysis of lamellar ruffling: effect of temperature change on human SH-SY5Y neuroblastoma cells. *J. Neurosci. Methods* **102**, 143–54.

32. Li, J. F. & Lowengrub, J. 2014 The effects of cell compressibility, motility and contact inhibition on the growth of tumor cell clusters using the Cellular Potts Model. *J. Theor. Biol.* **343**, 79–91. (doi:10.1016/j.jtbi.2013.10.008)

33. Kim, M.-C., Neal, D. M., Kamm, R. D. & Asada, H. H. 2013 Dynamic modeling of cell migration and spreading behaviors on fibronectin coated planar substrates and micropatterned geometries. *PLoS Comput. Biol.* **9**, e1002926. (doi:10.1371/journal.pcbi.1002926)

34. Hartmann-Petersen, R., Walmod, P. S., Berezin, A., Berezin, V. & Bock, E. 2000 Individual cell motility studied by time-lapse video recording: influence of experimental conditions. *Cytometry* **40**, 260–70.

35. Lepekhin, E. A., Walmod, P. S., Berezin, A., Berezin, V. & Bock, E. 2001 Evaluation of Cell Morphology. In *Cytoskeleton Methods and Protocols*, pp. 85–100. Humana Press.

36. Wegener, J., Seebach, J., Janshoff, a & Galla, H. J. 2000 Analysis of the composite response of shear wave resonators to the attachment of mammalian cells. *Biophys. J.* **78**, 2821–33. (doi:10.1016/S0006-3495(00)76825-1)

37. Wegener, J., Janshoff, a & Galla, H. J. 1999 Cell adhesion monitoring using a quartz crystal microbalance: comparative analysis of different mammalian cell lines. *Eur. Biophys. J.* **28**, 26–37.

38. Ferre-Pikal, E. S. et al. 1997 Draft revision of IEEE STD 1139-1988 standard definitions of physical quantities for fundamental, frequency and time metrology-random instabilities. In *Proceedings of International Frequency Control Symposium*, pp. 338–357. IEEE. [cited 2014 Jul. 2]. (doi:10.1109/FREQ.1997.638567)

39. Riley, W. J. 2008 *Handbook of Frequency Stability Analysis*. NIST Special Publication 1065.

40. Evans, E. A. & Calderwood, D. A. 2007 Forces and bond dynamics in cell adhesion. *Science* **316**, 1148–53. (doi:10.1126/science.1137592)

41. Tzvetkova-Chevolleau, T., Stéphanou, A., Fuard, D., Ohayon, J., Schiavone, P. & Tracqui, P. 2008 The motility of normal and cancer cells in response to the combined influence of the substrate rigidity and anisotropic microstructure. *Biomaterials* **29**, 1541–51. (doi:10.1016/j.biomaterials.2007.12.016)

42. Carlson, K. & Ehrich, M. 2000 Human neuroblastoma cell viability and growth are affected by altered culture conditions. *In Vitr. Mol. Toxicol.* **13**, 249–62.

43. Thurston, G. & Palcic, B. 1987 3T3 cell motility in the temperature range 33 degrees C to 39 degrees C. *Cell Motil. Cytoskeleton* **7**, 361–7. (doi:10.1002/cm.970070408)

44. Luchetti, F., Canonico, B., Della Felice, M., Burattini, S., Battistelli, M., Papa, S. & Falcieri, E. 2003 Hyperthermia triggers apoptosis and affects cell adhesiveness in human neuroblastoma cells. *Histol. Histopathol.* **18**, 1041–52.

45. Huang, S. H., Yang, K. J., Wu, J. C., Chang, K. J. & Wang, S. M. 1999 Effects of hyperthermia on the cytoskeleton and focal adhesion proteins in a human thyroid carcinoma cell line. *J. Cell. Biochem.* **75**, 327–37.

46. Remani, P., Ostapenko, V. V, Akagi, K., Bhattathiri, V. N., Nair, M. K. & Tanaka, Y. 1999 Relation of transmembrane potential to cell survival following hyperthermia in HeLa cells. *Cancer Lett.* **144**, 117–23.

Figure Captions

Figure 1. (A) Schematic of a quartz crystal Cr/AU top-surface (yellow), and **(B)** Cross-sectional schematic view of a SH-SY5Y human neuroblastoma cell adhering to the poly-L-lysine (PLL) coated crystal. (*Relative dimensions not to scale*)

Figure 2. (A) Frequency shift plots for two different surface coverages: 3.6% (surface coverage i) and 30.7% (surface coverage ii) of SH-SY5Y human neuroblastoma cells on different quartz crystals. Markers indicate the point of commencement in temperature increment of the flow-cell from 37 °C to 45 °C in order to apply heat shock to the adherent cells. Three different zones are also annotated which roughly define three different stages of the experiments. Zone 1 is where cells are healthy, Zone 2 is immediately after the temperature is increased and represents transition to cell apoptosis while Zone 3 is the stage just before the experiment is concluded with final stages of apoptosis. Increase in frequency in both the cases indicates decrease in mass loading (i.e. cell detachment from the surface) with time**. (B)-(C)** (*Two columns of three plots each*) are snapshots of frequency fluctuations in Zone 1, Zone 2 and Zone 3 (*top to bottom*) for the two cases of varying surface coverage. In all cases, the trend-line has been adjusted for representation purposes only. Notice that in the case of larger surface coverage, the signal is more "noisy" in Zone 2 while it is least in Zone 3. In the case of lower surface coverage, differences in the frequency fluctuations in three different zones are relatively smaller than the former case.

Figure 3. (A)-(B) Log-log overlapped Allan-deviation plots for the larger and smaller surface coverages respectively. From **(A)-(a)** it is quite evident that the fluctuation levels for all averaging times (τ) are highest for Zone 2, intermediate for Zone 1 while levels are lowest for Zone 3. This indicates when cells are alive, due to their activity, fluctuation levels are higher as copared to when cells are dead. Also, when cells are in a stressed state higher fluctuation levels are observed. **(A)-(b-d)-** Individual linear fitting curves (*black, continuous and slightly offset for clarity*) for three zones. Similarly, from **(B)-(a)** it is evident that while fluctuation levels for shorter averaging times are higher for both Zone 1 and Zone 2, fluctuation levels are only slightly higher for Zone 2. Linear fitting **(b-d)** indicate nature of noises (power-law type) for different zones as in the previous case.

Figure 4. (A)-(B) Log-log overlapped Allan-deviation plots for surface coverage iii (13%) and iv (22.5%) while **(C)-(D)** are Overlapped Allan-Deviation plots for control experiments. All the steps are common in control experiments with the exception of absence of any seed-ed cells. In **(C)**, surrounding media is DI water while in **(D)** surrounding media is cell culture.

Figure 5. (A)-(H) Phase-contrast optical images of cells seeded on a PLL coated glass surface. Temperature is increased from 37°C to 45°C over a period of 150 min during which cells changes morphology, ultimately shrink and become round which is characteristic of apoptosis.

Figure 6. (A)-(C) Phase-contrast images of SH-SY5Y cells at different time instances during the heating process. Coloured lines represent the tracks of various cells undergoing heat induced stress. In **(B),** arrows are indicating the direction of motion of individual cells while in **(C)** they are indicating the final positions of the cells. **(D)** Mean-square displacement plots of cells prior to the heat-stress phase of the experiment (first 16 minutes) indicating the presence of at least 2 categories of cell movements, fast and slow, while, a close fit to $MSD(\Delta t) = 4D\Delta t + (v\Delta t)^2$ is performed to extract diffusion coefficients and speed values. Similarly, **(E)** is MSD log-log plot for the last

stage of experiment (150^{th}-190^{th} minute). **(F)** Mean and standard deviation values for normalized change in the cell spreading (*apparent overlap area*) of the cells under consideration are plotted against time which peak almost half-way through and then rapidly decrease until the cells become spherical. **(G)** Total surface coverage shows a similar trend.